J. Cent. South Univ. (2023) 30: 3696−3708
DOI: https://doi.org/10.1007/s11771-023-5438-x

Springer

Non-isothermal aging behavior of a friction-surfaced Al-Cu-Mg alloy matrix composite coating reinforced by nickel-aluminide

Ramezanali FARAJOLLAHI[1], Hamed JAMSHIDI AVAL[1]*, Roohollah JAMAATI[1], Mousa JAVIDANI[2]

1. Department of Materials Engineering, Babol Noshirvani University of Technology, Shariati Avenue, Babol, 47148-71167, Iran;
2. Department of Applied Science, University of Québec at Chicoutimi, Saguenay, QC G7H 2B1, Canada

Abstract: This study investigates the effect of nickel-aluminide on Al-Cu-Mg alloys' non-isothermal aging behavior. The microstructure, mechanical properties, and corrosion resistance of nickel-aluminide-containing Al-Cu-Mg alloys were evaluated after non-isothermal aging treatment. The results show that the presence of nickel aluminide in the Al-Cu-Mg alloy changes the nature of S-Al_2CuMg precipitates to θ-Al_2Cu precipitates by adding 1.5 wt% Ni to the Al-Cu-Mg matrix. The non-isothermal aging treatment temperature for achieving the maximum mechanical properties during non-isothermal aging shifted from 250 ℃ to 300 ℃. Compared to isothermal artificial aging treatment at 170 ℃, the maximum hardness and mechanical properties increased by up to 9% in a nickel-aluminide containing Al-Cu-Mg alloy after non-isothermal aging treatment. The nickel-aluminide containing sample's maximum hardness and shear strength is $HV_{0.1}$(143.4±6.4) and (298.6±9.6) MPa, respectively occurring at 300 ℃. After non-isothermal aging treatment, the corrosion current intensity was reduced by approximately 58% and 49% in the nickel-containing coating compared to the AA2024 aluminum alloy substrate and coating without nickel-aluminide, respectively. Compared with the conventional artificial aging treatment, the corrosion current decreased by 16.7% more after non-isothermal aging treatment in the nickel-aluminide-containing coating.

Key words: non-isothermal aging; Ni additive; friction surfacing; microstructure; corrosion behavior

Cite this article as: Ramezanali FARAJOLLAHI, Hamed JAMSHIDI AVAL, Roohollah JAMAATI, Mousa JAVIDANI. Non-isothermal aging behavior of a friction-surfaced Al-Cu-Mg alloy matrix composite coating reinforced by nickel-aluminide [J]. Journal of Central South University, 2023, 30(11): 3696−3708. DOI: https://doi.org/10.1007/s11771-023-5438-x.

1 Introduction

Al-Cu-Mg alloys have long been used in various industries, especially in aerospace. Many efforts have been made to improve the properties and performance of this group of precipitation-hardened aluminum alloys for specific applications. One of the methods studied by researchers is to add alloying elements to this group of aluminum alloys [1 − 2]. Research has shown that adding nickel to aluminum alloys increases hardness, tensile properties, wear resistance, and thermal stability due to the formation of nickel-aluminide intermetallic compounds (IMCs) [3 − 5]. Considering these conditions, Al-Cu-Mg alloys' coatings containing nickel can improve the performance of components exposed to high temperatures, at which they should maintain mechanical and wear resistance. There are various methods for applying the coating [6 − 8],

Received date: 2023-02-07; **Accepted date:** 2023-07-31
Corresponding author: Hamed JAMSHIDI AVAL, PhD, Associate Professor; E-mail: h.jamshidi@nit.ac.ir; ORCID: https://orcid.org/0000-0002-5431-0413

among which solid-state methods have a special place because they create a thick layer with a strong metallurgical bond and do not have the defects of conventional melting methods [9]. One of the solid-state coating methods is friction surfacing (FS), which uses a rotating consumable rod that is affected by a vertical force and moves the substrate surface to apply the coating [10].

Recent research has shown that one way to simultaneously improve mechanical properties and reduce corrosion of age-hardenable aluminum alloys is to perform non-isothermal aging (NIA) heat treatment instead of isothermal aging (IA) heat treatment. Based on available sources, most NIA studies on aluminum alloys focus on Al-Mg-Si and Al-Zn-Mg-Cu alloys [11 − 20]. ZHAN et al [21] studied the effect of NIA treatment on Al-Cu-Mg-Si alloy mechanical properties, microstructure, and corrosion behavior. They reported that NIA treatment increased corrosion resistance by reducing the precipitate-free zone (PFZ) and the interconnection between precipitates at the grain boundary. It was also reported that the tensile strength and yield strength of the alloy after NIA treatment increased by 1.5% and 5.8%, respectively, compared to those after IA heat treatment. ZHOU et al [22] studied the effect of NIA treatment on Al-Zn-Mg-Cu alloy stress corrosion cracking (SCC) behavior. They showed that NIA treatment significantly increased SCC resistance compared to conventional T6 and T77 heat treatments. KE et al [23] investigated the effect of NIA treatment on Al-Zn-Mg alloy mechanical and electrical properties. The results showed that NIA treatment caused a 9.7% increase in mechanical properties compared to T6 treatment. It also caused a significant improvement in electrical properties compared to T73 heat treatment. SEPEHRBAND et al [24] investigated the effect of NIA treatment on Al-Mg-Si alloys. The results showed that the initial precipitates formed during heat treatment prevented dynamic deformation or static recovery during the early annealing stages.

According to available sources, the effect of NIA treatment on Al-Cu-Mg alloys containing nickel-aluminide has not been investigated so far. Although nickel aluminides increase the thermal stability and corrosion resistance of the aluminum matrix [25 − 29], adding nickel to Al-Cu-Mg alloys and the formation of nickel aluminides can result in copper adsorption in the microstructure [30], which can affect the aging behavior of these alloys. There is no investigation into the effect of Al-Ni intermetallic reinforcement on the microstructure and corrosion behavior of an Al-Cu-Mg aluminum alloy coating following NIA treatment. In this research, the AA2024 substrate was cladded with an Al-Cu-Mg alloy containing 1.5 wt% nickel aluminides using the FS process. Then, the effect of NIA treatment on coating microstructure, mechanical properties, and corrosion resistance was investigated. The effect of NIA treatment on the corrosion behavior of the coating was also compared with the coating treated with isothermal aging heat treatment.

2 Materials and methods

In this study, the FS was performed on an Al-Cu-Mg alloy substrate with a thickness of 2 mm. The composition and mechanical properties are mentioned in Tables 1 and 2. The coating was performed using an AA2024 aluminum alloy rod containing 1.5 wt% nickel aluminide. To make the AA2024 mechtrod containing nickel aluminide, AA2024 alloy was melted according to the chemical composition mentioned in Table 1, and 1.5 wt% nickel powder was added to the molten aluminum using the setup presented in Figure 1.

Table 1 Chemical composition of mechtrod and substrate alloys wt%

Alloy	Si	Fe	Cu	Mn	Mg	Al
Mechtrod	0.14	0.26	4.14	0.49	1.45	Bal.
Substrate	0.18	0.25	3.21	0.40	1.35	Bal.

Nickel powder with an approximate size of 5 − 75 μm and 99.9% purity was used as reinforcement. In the mechtrod fabrication process, various equipments such as the electric furnace, graphite crucible, electric motor for stirring molten aluminum, Al_2O_3-coated steel impeller, thermocouple, and reinforcement powder injection system were used. The mechtrod manufacturing process begins with preheating the crucible in an electric furnace.

Then, hexachloroethane (C_2Cl_6) tablets are used for degassing the molten aluminum; the slag is removed. Afterward, the stirrer is introduced into

Table 2 Mechanical properties of mechtrod and substrate alloys

Alloy	Ultimate tensile strength/MPa	Yield strength/MPa	Elongation/%	Hardness (HV)
Mechtrod	435.76±9.03	311.45±8.94	18.02±1.43	136.43±6.13
Substrate	425.91±10.02	304.78±9.32	19.34±2.04	131.13±4.01

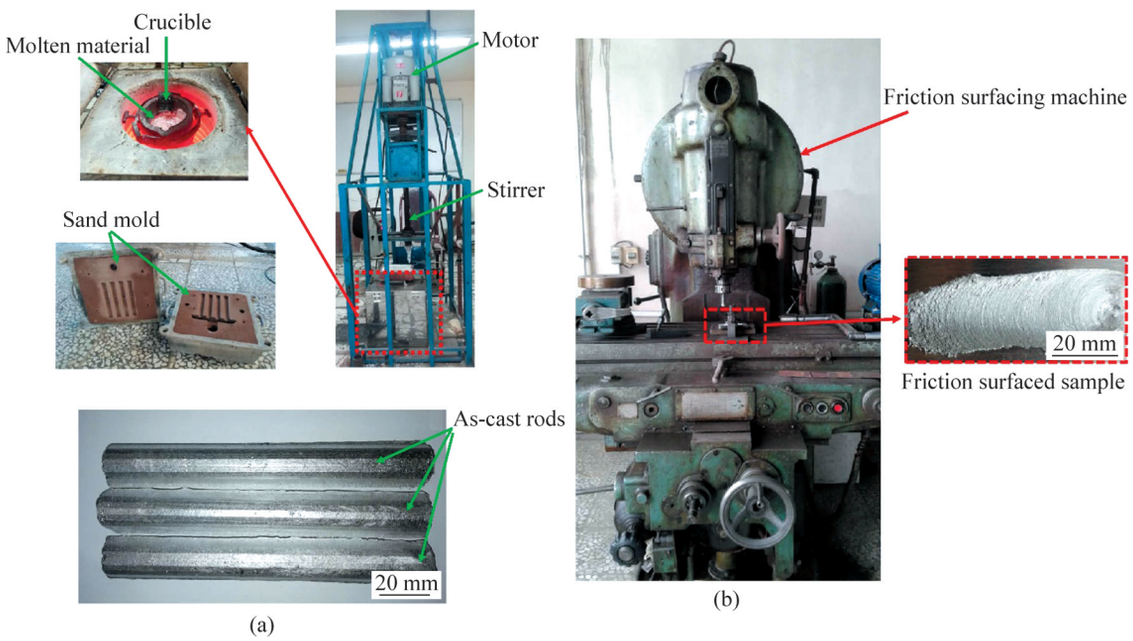

Figure 1 (a) Experiment setup for fabrication of aluminum rod containing nickel-aluminide; (b) Friction surfacing equipment

the molten aluminum, and the stirring operation is performed with an electric motor equipped with a speed-adjustment system. In this procedure, argon is initially introduced into the furnace at a pressure of 3.5 bar. Nickel powder is added to the furnace at the inlet argon gas pressure (3.5 bar). After completing the nickel powder injection (for 8 min), stirring is continued for 2 min to ensure the reaction is made between the nickel powder and the aluminum alloy.

This process is accomplished by efficiently distributing the nickel powder in molten aluminum. Finally, the crucible is removed from the furnace, and molten materials are poured into a sand mold with a diameter of 22 mm and a length of 200 mm. Then, the AA2024-1.5 wt% nickel aluminide mechtrod with a diameter of 20 mm and a length of 100 mm was prepared through machining. According to preliminary studies on process parameters that lead to the highest coating efficiency, the coating operation was performed with a rotational speed of 600 r/min, a traverse speed of 100 mm/min, and an axial feeding rate of 95 mm/min using rods with and without nickel-aluminide. To investigate the behavior of the coat concerning NIA treatment, first, the coatings were subjected to solid solution treatment at 500 ℃ for 2 h. Then, NIA treatment was performed on solid solutionized samples with a 10 ℃/min heating rate. After reaching the temperature of the sample to 100, 150, 200, 250, 300, 350 and 400 ℃, the heat-treated sample was removed from the furnace, and after quenching in water at a temperature of 25 ℃, the microstructure, hardness, and shear strength were evaluated. For each temperature one sample is heat treated. Moreover, an isothermal aging treatment was performed on solid solutionized coatings at 170 ℃ for 12 h.

After coating, different samples were collected to evaluate the coating microstructure, mechanical properties, and corrosion resistance. The microstructure of the coated samples was studied using an optical microscope (DG Victory-Dewinter), scanning electron microscope (SEM), and transmission electron microscopy (TEM) (Oxford Instruments). The TEM samples were prepared by hand grinding and polishing to a thickness of approximately 30 − 50 μm, then ion milling to a thickness suitable for observation under

a TEM microscope. The ion milling was performed using an accelerating voltage of 2−4 keV at an angle of 3° to the surface. Clemex Vision image analyzers were used in this study to measure gain and precipitate sizes. Image analysis was performed on at least ten images related to each sample.

The hardness of the samples was measured using the micro-Vickers hardness test according to ASTM E92 using a 100 gr load for a dwell time of 10 s. Shear punch tests (SPT) were conducted to measure the mechanical properties of the coated samples and consumable rods. The 1 mm-thick slices of the materials were ground to 0.7 mm, from which disks of 10 mm diameter were punched for SPT. A shear punch fixture with a 3.175 mm diameter flat cylindrical punch and a 3.225 mm diameter receiving hole, as shown in Figure 2, was used for SPT. All shear punch tests were performed at room temperature with a punch speed of 0.001 mm/s. Electrochemical tests were performed to evaluate coating corrosion resistance. All experiments were carried out using the CS350 electrochemical workstation. Before each test, the samples were immersed in NaCl solution for 1 h to achieve steady-state conditions. In the polarization tests, the samples were polarized at 250 mV below the open circuit potential at a scanning rate of 1 mV/s.

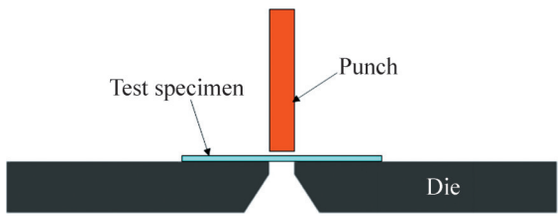

Figure 2 Schematic of shear punch test

3 Results and discussion

Figure 3 depicts the macrograph of the two coatings and the microstructure of different zones of the coatings. The coating efficiency of samples with and without nickel aluminide was calculated at 56.32% and 58.27%, respectively, using the equations presented in Ref. [31]. According to the previous study [5], the hardness of the two mechtrods with and without nickel aluminide was HV (115.36±8.32) and HV (116.08±5.57), respectively. Moreover, the yield strengths of rods

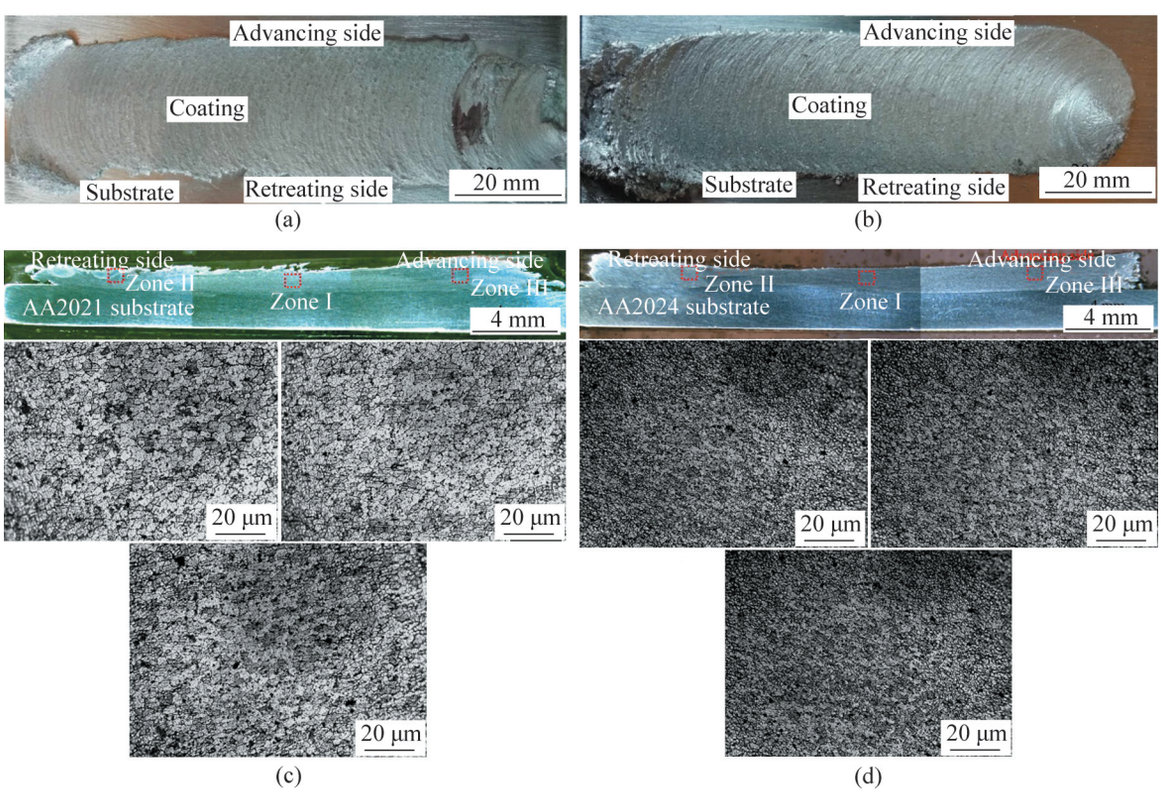

Figure 3 (a) Macrograph of nickel-aluminide free sample; (b) Macrograph of nickel-aluminide containing sample; Macrostructure and microstructure of different zones of (c) nickel-aluminide free sample, and (d) sample containing nickel-aluminide

with and without nickel aluminide were (183.51±6.32) and (162.08±9.48) MPa, respectively. As the strength of the mechtrod increases, higher torque is required to create a viscoplastic layer at the tip of the mechtrod.

Therefore, it can be expected that with the rise in the strength of the mechtrod, given the constant coating process parameters, the formation of a viscoplastic layer at the tip of the mechtrod would be more difficult. As a result, plastic material is created in a smaller volume at the tip of the mechtrod. This reduces the coating's dimensions and thickness, ultimately lowering its efficiency.

On the other hand, the temperature measurements at the coating-substrate interface showed that the temperatures in the coating with and without nickel aluminide were 227 ℃ and 255 ℃, respectively. Therefore, it can be expected that larger plastic deformation occurs in a mechtrod with lower strength. This can increase the heat generated by plastic deformation and friction [32]. As the temperature increases, the mechtrod strength decreases, leading to larger plastic deformation. Nevertheless, it should be noted that reduced dimensions, and thus, the lower efficiency of the coating with the rise in the strength of the mechtrod, have been reported in Refs. [31, 33].

The nickel-containing and nickel-free samples had average grain sizes of (2.1±0.7), and (3.9±0.6) μm, respectively. All coatings exhibited fine equiaxed grains formed due to dynamic recrystallization [34]. HUMPHREYS and HATHERLY [35] found that temperature and plastic strain rate strongly affect recrystallized grain size. The recrystallized grain size decreases with a reduction in the temperature and a rise in the plastic strain rate. And the plastic strain rate ($\dot{\varepsilon}$) in the coated samples can be calculated using the geometric coating and friction surfacing parameters [31]. Accordingly, the plastic strain rates of samples with and without nickel aluminide are 987 s^{-1} and 1032 s^{-1}, respectively. The grain size distribution of samples coated with nickel-aluminide-free rods indicates that grain growth capability is predominant despite the higher plastic strain rate in these samples due to the higher coating temperature. These coatings have larger grain sizes.

The microstructural changes of as-cast rods and the central zones of the coatings before NIA in different samples were investigated using SEM and EDS analyses, whose results are shown in Figure 4.

According to the EDS point analysis (Figure 5 and Table 3) of the consumable rod and coated samples without nickel aluminide, precipitates, and secondary phase particles are S-Al_2CuMg, Al_7Cu_2Fe, and Fe-rich particles. According to previous works

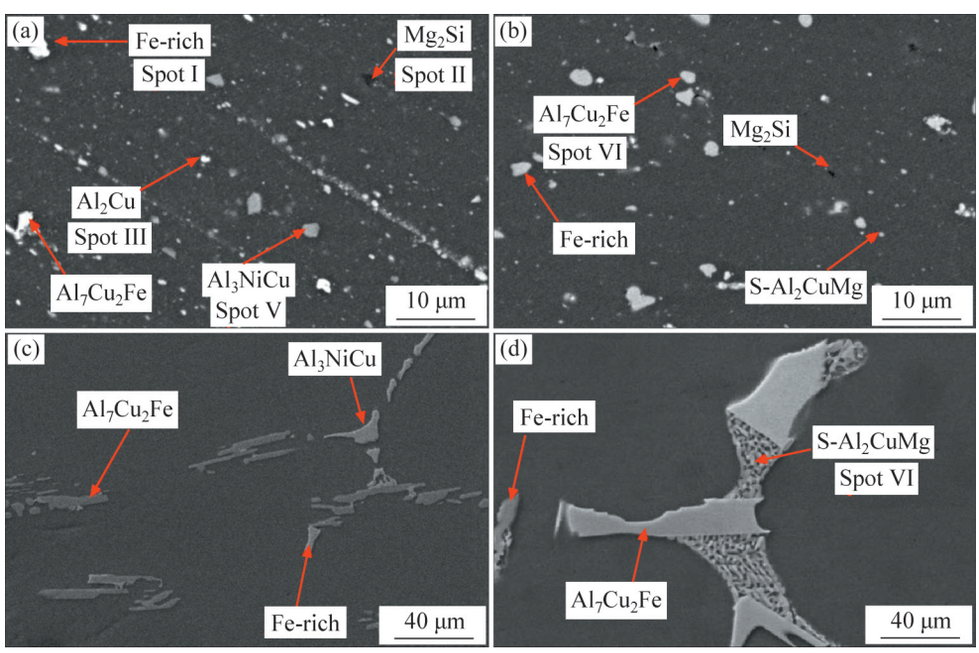

Figure 4 SEM micrograph of precipitates and second-phase particles at center of coatings: (a) Nickel-aluminide containing sample; (b) Nickel-aluminide free sample; (c) Mechtrod containing nickel-aluminide; (d) Mechtrod without nickel-aluminide

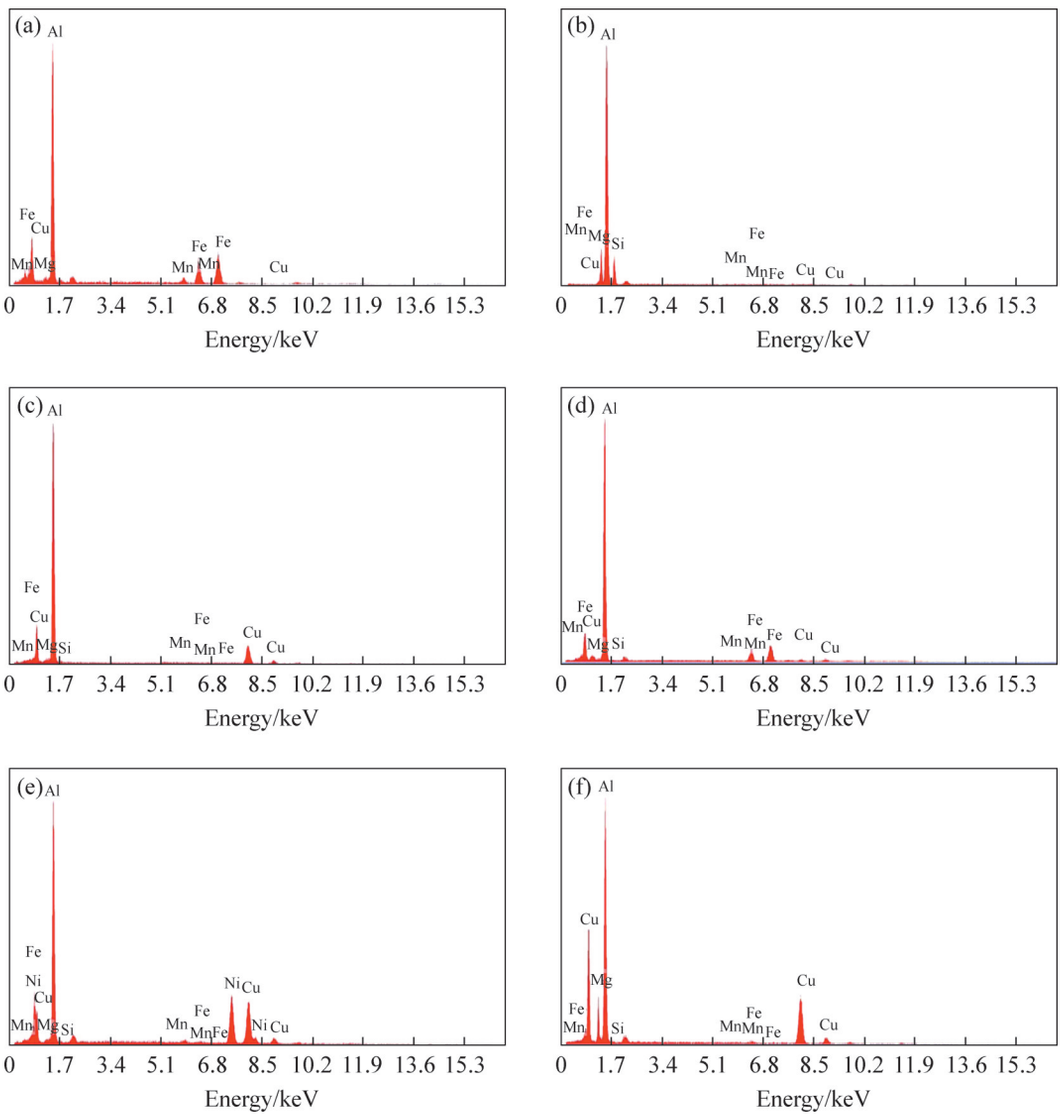

Figure 5 EDS results of points marked in the Figure 4: (a) Spot I; (b) Spot II; (c) Spot III; (d) Spot IV; (e) Spot V; (f) Spot VI

Table 3 Chemical composition of different points marked in Figure 4 at%

Position	Al	Fe	Cu	Mn	Mg	Si	Ni
I	74.08	15.12	0.12	10.21	0.23	0.24	—
II	80.12	0.13	0.05	0.12	13.56	6.02	—
III	85.59	0.05	14.12	0.04	0.09	0.11	—
IV	85.77	5.32	8.65	0.04	0.09	0.13	—
V	68.61	0.02	16.89	0.05	0.07	0.04	14.32
VI	63.2	0.07	19.43	0.05	17.21	0.04	—

[5, 36] and XRD analysis, similar phases were found. However, in the rod and coated sample containing nickel aluminide, Al_3NiCu particles, and θ-Al_2Cu and Mg_2Si are visible in addition to the Al_7Cu_2Fe, Fe-rich secondary phase particles. As can be seen, S-Al_2CuMg precipitates have disappeared, and θ-Al_2Cu and Mg_2Si precipitates have been formed.

Based on the EDS analysis of the coated samples, after solid solution heat treatment, copper concentrations in nickel-containing and nickel-free samples were obtained at 1.9 at% and 3.1 at%, respectively. Therefore, it can be said that the addition of nickel reduces the concentration of copper in the matrix due to the adsorption of copper atoms. This reduces the formation of S-Al_2CuMg precipitates in the coating containing nickel. In other words, it can be said that by reducing the ratio of copper to magnesium in the aluminum matrix, the copper in the matrix has precipitated in the form of θ precipitate, and magnesium has also appeared

in the form of Mg_2Si.

After solid solution heat treatment of the two samples, NIA heat treatment at a heating rate of 10 ℃ was performed on the coated samples. Figure 6 shows hardness and shear strength measurement results. As can be seen, with the rise in temperature, hardness and strength increase and decrease. The nickel-free sample's maximum hardness and shear strength are $HV_{0.1}$(154.3±5.3) and (305.5±8.9) MPa, respectively, occuring at 250 ℃. However, the maximum hardness and shear strength are $HV_{0.1}$(143.4±6.4) and (298.6±9.6) MPa, respectively in the sample containing nickel occuring at 300 ℃. The lower hardness and strength of the nickel-containing sample and achieving the maximum hardness and strength at higher temperatures are probably due to the effect of nickel on reducing the formation of S precipitates in the Al-Cu-Mg alloy. However, as shown in Figure 6, both coatings show higher hardness and strength after isothermal aging and NIA treatment.

Another important point is the high thermal stability of the nickel-containing coating. This means that the hardness reduction rate in a nickel-free sample after reaching the maximum hardness is HV0.33/℃, but in the sample containing nickel, the hardness reduction rate after reaching the maximum hardness equals HV0.13/℃. A similar trend can be seen in the shear strength results. Figure 7 shows the grain size distribution of coatings with the maximum hardness after NIA and isothermal aging treatment.

The average grain size of the nickel-containing coating after NIA and IA treatments is (89.2±10.1)

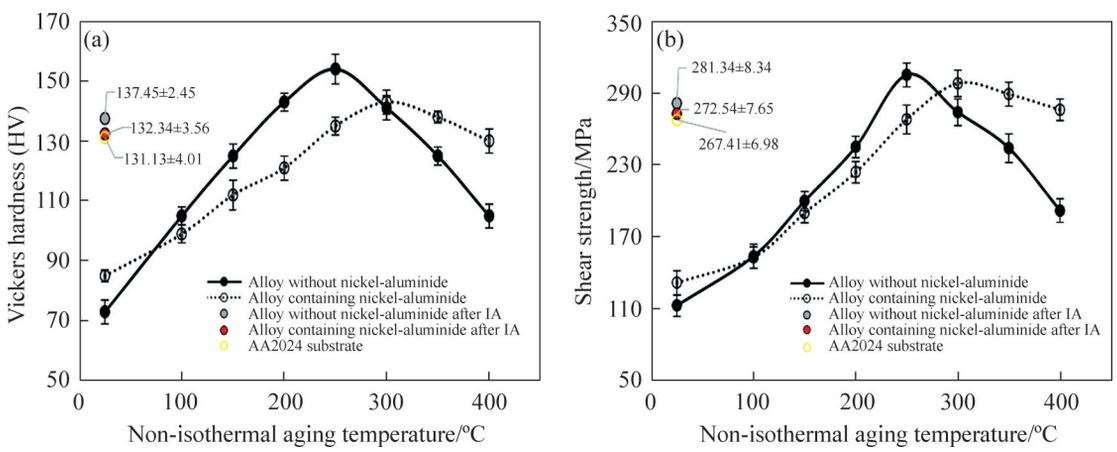

Figure 6 Variation of (a) average hardness and (b) shear strength of different samples versus non-isothermal aging treatment temperature (The hardness and shear strength after IA treatment reported as a point in the graphs)

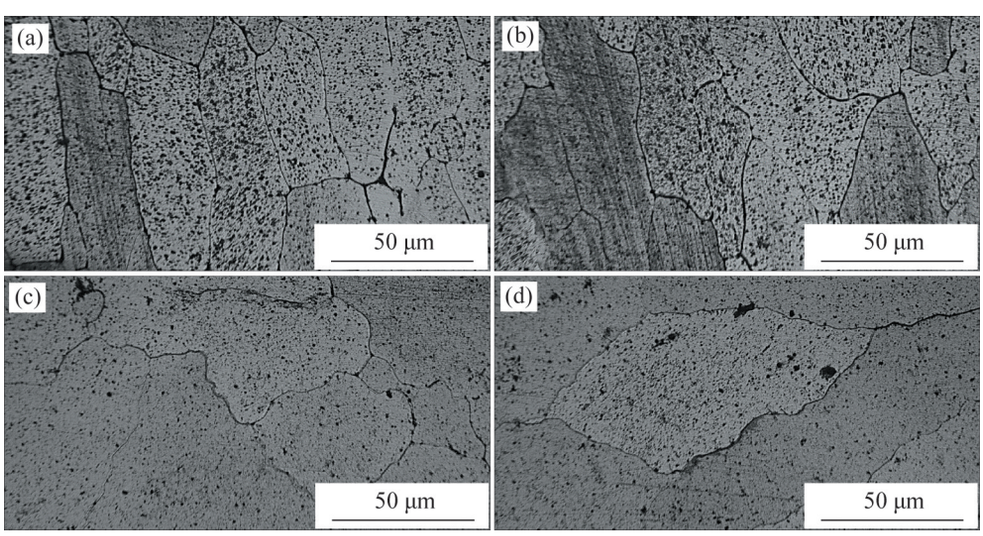

Figure 7 Microstructure of center zone of coated samples after heat treatment: (a) Nickel-aluminide containing sample after NIA; (b) Nickel-aluminide containing sample after IA treatment; (c) Nickel-aluminide free sample after NIA; (d) Nickel-aluminide free sample after IA treatment

and (93.4±9.7) μm, respectively. Meanwhile, the average grain sizes of the nickel-free coating after NIA and IA treatments are (145.9±7.1) and (150.1±10.2) μm, respectively. The average grain size of coatings after NIA and IA treatments is almost the same. As can be seen, all coatings have experienced significant grain growth. Although the grain size is smaller in nickel-aluminide coatings, abnormal grain growth (AGG) is observed in all coatings. Various factors such as anisotropy in grain boundary mobility and energy, reduction of barrier force on grain boundary due to the growth or dissolution of precipitates or second-phase particles, and thermodynamic driving force due to grain size distribution can affect AGG. AGG has also been observed following heat treatment in previous studies [37 − 39], where a fine recrystallized microstructure is created via friction stir processes. Notably, nickel-aluminide intermetallic acts as a grain growth barrier, preventing it to a large extent.

To more precisely examine the nature and type of precipitates formed in the coatings, TEM images of the coatings before NIA, coatings with maximum hardness after NIA, and coatings after IA treatment are shown in Figure 8. The microstructure of the coated samples before NIA and IA heat treatments confirms the SEM results. Al_3NiCu particles can also be seen in the nickel-containing coating. The formation of round S-Al_2CuMg and rod shape θ-Al_2Cu precipitates in the nickel-free and nickel-containing coating is quite evident. Their average size in the coating with and without nickel is (102.5±7.3) and (112.4±8.5) nm, respectively. The image analysis performed on TEM images shows that the area ratio of S-Al_2CuMg and θ-Al_2Cu precipitates is 0.032 and 0.019, respectively. The microstructure of the coating after the NIA and IA heat treatment processes shows that the type and morphology of precipitates and second-phase particles do not change, but the size of S-Al_2CuMg and θ-Al_2Cu precipitates and their concentration change according to the heat treatment conditions. The concentration of strengthening precipitates S-Al_2CuMg and θ-Al_2Cu, regardless of the type of heat treatment, is lower in the nickel-containing coating. Although the concentration (area ratio) of these precipitates does not change much after NIA and IA treatments, the size of precipitates in the samples undergoing NIA treatment is finer than in the samples undergoing IA treatment. In the coating containing nickel-aluminide, the average size of θ-Al_2Cu precipitates after NIA and IA treatment is (69.3±7.2) and (74.8±6.4) nm, respectively. Besides, in the nickel-aluminide-free coating, the average size of S-Al_2CuMg precipitates after NIA and IA treatment is (65.9±5.7) and (68.4±6.3) nm, respectively.

The effect of NIA and IA heat treatment on the polarization curve of the coated samples, the substrate, and the mechtrod is shown in Figure 9. Figure 10 reports corrosion current, voltage, and resistance results. According to the polarization test results, it can be concluded that regardless of nickel aluminide, NIA and IA treatments will improve polarization resistance. Of course, it should be noted that the presence of nickel aluminide and the NIA treatment causes a significant change in polarization results. This is due to the improvement of polarization resistance. According to the microstructural results, it may be possible to attribute the significant improvement in corrosion resistance in the nickel-containing coating after NIA treatment to the formation of θ precipitates and nickel-aluminide compounds. Corrosion begins with Cl^- ions attacking the oxide surface. The ions accumulate instead of secondary phases, precipitate with a weak protective layer, and destroy the oxide layer.

Next, a microgalvanic cell is formed between Al and S, θ and nickel-rich precipitates and compounds, and corrosion changes from chemical to electrochemical. The θ and S precipitates have a more negative potential than the aluminum matrix. They accept the role of anode and corrode. It seems that the presence of nickel-rich particles, as reported in Ref. [40], could give a complete protective role to θ precipitates than S precipitates. Of course, it should be noted that several factors, such as the formation of fine precipitates [41−42], the reduction of residual stresses caused by heat treatment, and the reduction of grain boundary density, can all contribute to the coating's corrosion resistance. The Nyquist plots reported in Figure 11 exhibiting capacitive loops, also reflected in the Bode impedance plots. This reveals the formation of an oxide layer on the surface in the chloride solution environment. The corrosion process of extruded samples can be explained using equivalent circuits

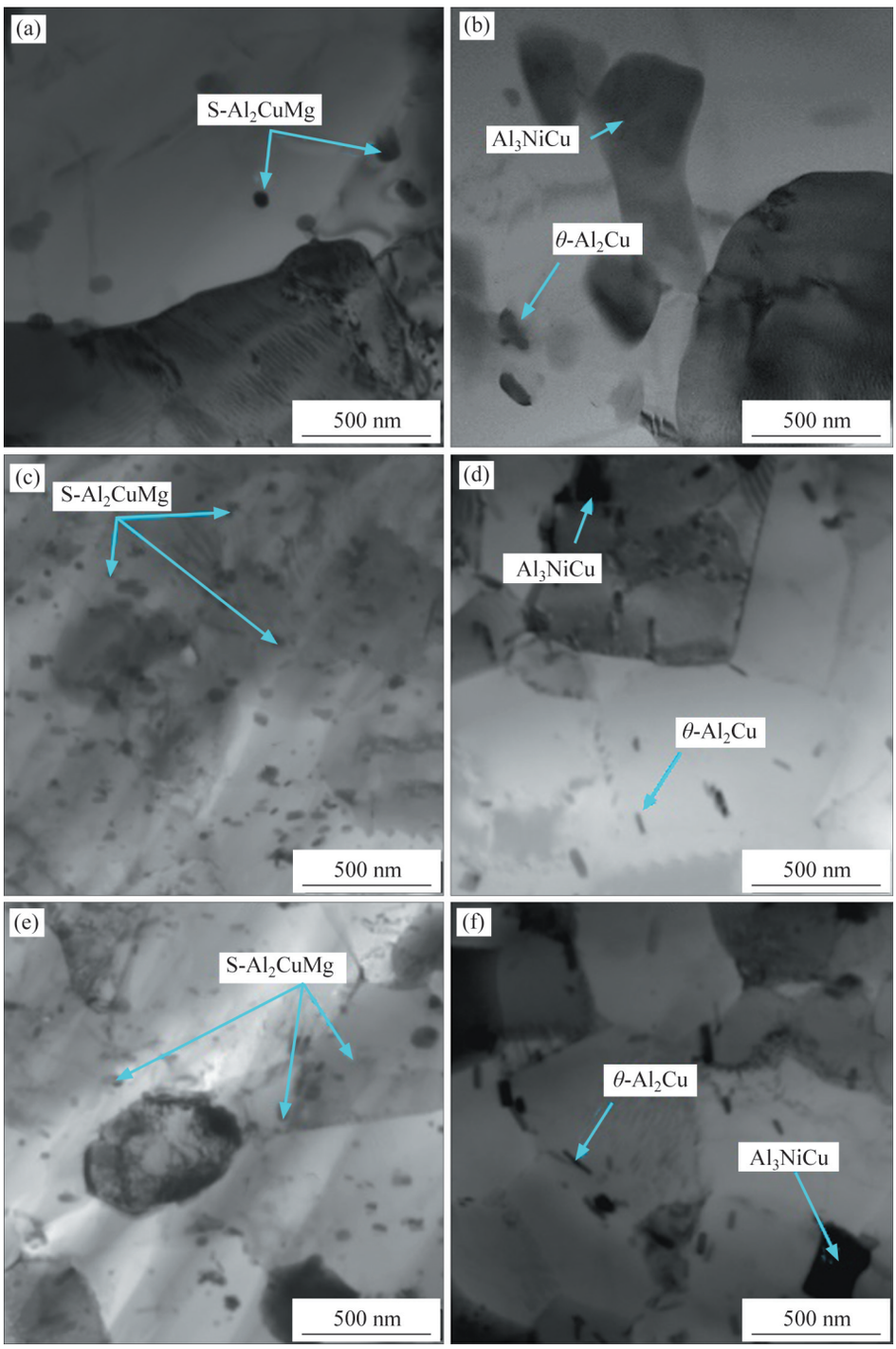

Figure 8 TEM images of different samples: (a) Nickel-aluminide free sample before aging; (b) Nickel-aluminide containing sample before aging; (c) Nickel-aluminide free sample after IA treatment; (d) Nickel-aluminide containing sample after IA treatment; (e) Nickel-aluminide free sample after NIA treatment; (f) Nickel-aluminide containing sample after NIA treatment

reported in Ref. [43].

Based on the fitting parameters, the greatest corrosion resistance is related to nickel-containing coating after NIA treatment. Figure 11 displays the samples' phase curves. Each sample exhibits a consistent decline in phase angle, indicating the presence of a passivation layer. In addition, it exhibits a decline in protective properties with time and frequency. The highest and greatest phase angle indicate considerable electrochemical resistance and further support the creation of a high-density oxide film.

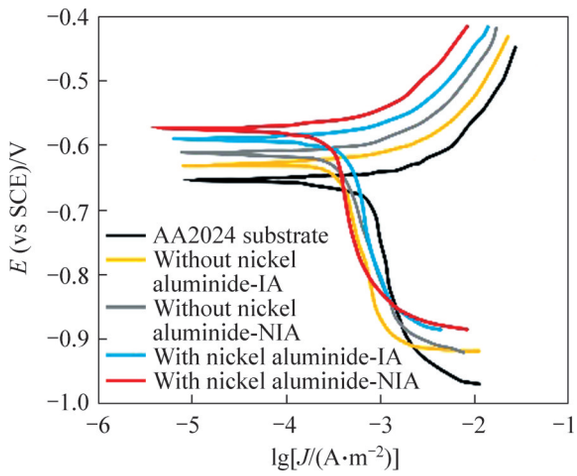

Figure 9 Polarization curve of different samples

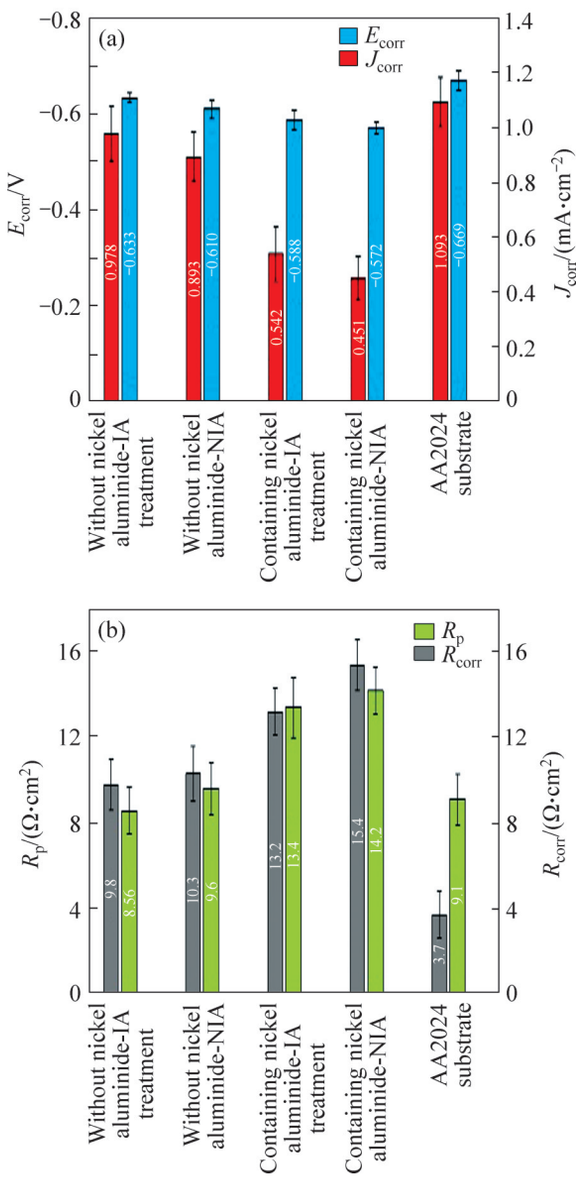

Figure 10 (a) Corrosion current (J_{corr}) and corrosion voltage (E_{corr}); (b) Polarization resistance (R_p) and corrosion resistance (R_{corr}) of different samples

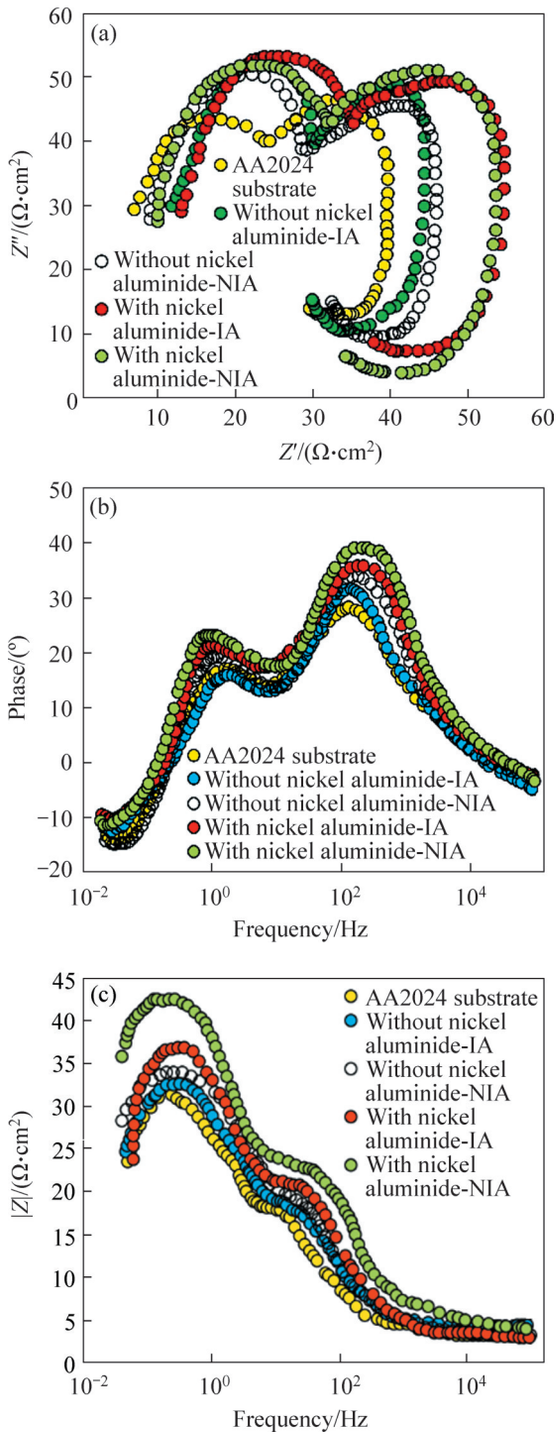

Figure 11 EIS results of different samples; (a) Nyquist plots; (b) Phase plots; (c) Bode plots of EIS plots

4 Conclusions

This study investigated the effect of NIA treatment on the microstructure, mechanical properties, and corrosion behavior of an Al-Cu-Mg alloy coating reinforced with 1.5 wt% nickel-aluminide. The main findings are as follows:

1) Due to the adsorption of copper atoms by nickel-aluminide in the Al-Cu-Mg alloy, the S-Al_2CuMg precipitation ability decreased, such that by adding 1.5 wt% Ni to the Al-Cu-Mg matrix, the peak of maximum mechanical properties during non-isothermal aging shifted from 250 ℃ to 300 ℃.

2) A comparison between the coatings' mechanical properties after artificial aging and NIA treatment revealed the higher hardness of both coatings with and without nickel-aluminide after NIA treatment.

3) During the NIA treatment, the hardness reduction rates in the nickel-free and nickel-containing samples were HV0.33/℃ and HV0.13/℃, respectively, after reaching the maximum hardness.

4) The average grain size of coatings after NIA and IA treatments was almost the same. Moreover, nickel-aluminide intermetallic acted as a grain growth barrier, preventing it to a large extent.

5) In both coated samples with and without nickel-aluminide, corrosion current decreased after NIA and IA heat treatments. Besides, compared to the IA treatment, the corrosion current decreased by 16.7% more after the NIA treatment in the nickel-aluminide-containing coating.

Contributors

Ramezanali FARAJOLLAHI participated in investigation, resources, and writing the original draft. Hamed JAMSHIDI AVAL participated in conceptualization, methodology, writing-review & editing, and supervision. Roohollah JAMAATI participated in conceptualization, methodology, writing-review & editing, and supervision. Mousa JAVIDANI participated in conceptualization, methodology, writing-review & editing, and supervision.

Conflict of interest

Ramezanali FARAJOLLAHI, Hamed JAMSHIDI AVAL, Roohollah JAMAATI, and Mousa JAVIDANI declare that they have no conflict of interest.

References

[1] ABDO H S, SEIKH A H, MOHAMMED J A, et al. Alloying elements effects on electrical conductivity and mechanical properties of newly fabricated Al based alloys produced by conventional casting process [J]. Materials, 2021, 14(14): 3971. DOI: 10.3390/ma14143971.

[2] GUO Xin-peng, LI Hui-jun, PAN Zeng-xi, et al. Microstructure and mechanical properties of ultra-high strength Al-Zn-Mg-Cu-Sc aluminum alloy fabricated by wire + arc additive manufacturing [J]. Journal of Manufacturing Processes, 2022, 79: 576−586. DOI: 10.1016/j.jmapro.2022.05.009.

[3] LIU Fu-chu, ZHU Xiang-zhen, JI Shou-xun. Effects of Ni on the microstructure, hot tear and mechanical properties of Al-Zn-Mg-Cu alloys under as-cast condition [J]. Journal of Alloys and Compounds, 2020, 821: 153458. DOI: 10.1016/j.jallcom.2019.153458.

[4] NATH OP A R, ARUL S. Effect of nickel reinforcement on micro hardness and wear resistance of aluminium alloy Al7075 [J]. Materials Today: Proceedings, 2020, 24: 1042−1051. DOI: 10.1016/j.matpr.2020.04.418.

[5] FARAJOLLAHI R, JAMSHIDI AVAL H, JAMAATI R. Effects of Ni on the microstructure, mechanical and tribological properties of AA2024-Al_3NiCu composite fabricated by stir casting process [J]. Journal of Alloys and Compounds, 2021, 887: 161433. DOI: 10.1016/j. jallcom.2021.161433.

[6] THAKARE J G, PANDEY C, MAHAPATRA M M, et al. Thermal barrier coatings—A state of the art review [J]. Metals and Materials International, 2021, 27(7): 1947−1968. DOI: 10.1007/s12540-020-00705-w.

[7] THAKARE J G, PANDEY C, MULIK R S, et al. Mechanical property evaluation of carbon nanotubes reinforced plasma sprayed YSZ-alumina composite coating [J]. Ceramics International, 2018, 44(6): 6980 − 6989. DOI: 10.1016/j.ceramint.2018.01.131.

[8] KANWAL S, THAKARE J G, PANDEY C, et al. Characterization of slurry-based mullite coating deposited on P91 steel welds [J]. Journal of the Australian Ceramic Society, 2019, 55(2): 519 − 528. DOI: 10.1007/s41779-018-0258-4.

[9] TUNCER N, BOSE A. Solid-state metal additive manufacturing: A review [J]. JOM, 2020, 72(9): 3090−3111. DOI: 10.1007/s11837-020-04260-y.

[10] BARARPOUR S M, JAMSHIDI AVAL H, JAMAATI R. Effects of Zn powder on alloying during friction surfacing of Al-Mg alloy [J]. Journal of Alloys and Compounds, 2020, 818: 152823. DOI: 10.1016/j.jallcom.2019.152823.

[11] KE Bin, YE Ling-ying, ZHANG Yong, et al. Enhanced mechanical properties and corrosion resistance of an Al-Zn-Mg aluminum alloy through variable-rate non-isothermal aging [J]. Journal of Alloys and Compounds, 2022, 890: 161933. DOI: 10.1016/j.jallcom.2021.161933.

[12] ZHAO Hui, YE Ling-ying, CHENG Quan-shi, et al. Effect of variable rate non-isothermal aging on microstructure and properties of Al-Zn-Mg-Cu alloy [J]. Materials Characterization, 2023, 197: 112715. DOI: 10.1016/j.matchar.2023.112715.

[13] YANG Jie, LIU Hong-feng, ZENG Tao, et al. Effect of non-isothermal aging on the mechanical properties and corrosion resistance of 2A12 aluminum alloy [J]. Materials, 2023, 16(11): 3921. DOI: 10.3390/ma16113921.

[14] ZHAO Hui, YE Ling-ying, CHENG Quan-shi, et al. Enhanced mechanical properties and corrosion resistance of 7055 aluminum alloy through variable-rate non-isothermal aging [J]. Journal of Alloys and Compounds, 2023, 943: 169198. DOI: 10.1016/j.jallcom.2023.169198.

[15] WANG Jian, XIE Jing-pei, MAO Zhi-ping, et al. Microstructure evolution and mechanical properties of the Al-Cu-Mg-Ag alloy during non-isothermal aging [J]. Journal of Alloys and Compounds, 2023, 942: 169031. DOI: 10.1016/j.jallcom.2023.169031.

[16] YANG Xian-wen, CHENG Quan-shi, DONG Yu, et al. Effect of various non-isothermal aging on properties and microstructure of 7055 aluminum alloy [J]. Journal of Materials Research and Technology, 2023, 25: 6275−6287. DOI: 10.1016/j.jmrt.2023.07.068.

[17] TANG Cheng-lu, LUO Bing-hui, BAI Zhen-hai, et al. Effect of non-isothermal ageing on microstructure and mechanical properties of an Al-Cu-Mg-Ag alloy [J]. Materials Science and Engineering A, 2022, 830: 142315. DOI: 10.1016/j.msea.2021.142315.

[18] FARAJOLLAHI R, JAMSHIDI AVAL H, JAMAATI R. Non-isothermal aging behavior of in situ AA2024 − Al_3NiCu composite [J]. Transactions of Nonferrous Metals Society of China, 2022, 32(7): 2125−2137. DOI: 10.1016/S1003-6326(22)65935-1.

[19] ZANG Chen-yang, XIAO Wen-long, FU Yu, et al. Enhanced properties and homogeneity of Al-Zn-Mg-Cu alloy thick plate by non-isothermal aging [J]. Journal of Alloys and Compounds, 2023, 952: 170023. DOI: 10.1016/j.jallcom.2023.170023.

[20] REZAEI M, AVAL H J. Effect of Cu/Mg ratio on microstructure and corrosion resistance of Al-Cu-Mg-Li cast alloy during non-isothermal aging [J]. Metals and Materials International, 2023, 29(7): 1907−1922. DOI: 10.1007/s12540-022-01363-w.

[21] ZHAN Xin, TANG Jian-guo, LI Hui-zhong, et al. Effects of non-isothermal aging on mechanical properties, corrosion behavior and microstructures of Al-Cu-Mg-Si alloy [J]. Journal of Alloys and Compounds, 2020, 819: 152960. DOI: 10.1016/j.jallcom.2019.152960.

[22] ZHOU Liang, CHEN Kang-hua, CHEN Song-yi, et al. Correlation between stress corrosion cracking resistance and grain-boundary precipitates of a new generation high Zn-containing 7056 aluminum alloy by non-isothermal aging and re-aging heat treatment [J]. Journal of Alloys and Compounds, 2021, 850: 156717. DOI: 10.1016/j.jallcom.2020.156717.

[23] KE Bin, YE Ling-ying, ZHANG Yong, et al. Enhanced strength and electrical conductivities of an Al-Zn-Mg aluminum alloy through a new aging process [J]. Materials Letters, 2021, 304: 130586. DOI: 10.1016/j.matlet.2021.130586.

[24] SEPEHRBAND P, WANG X, JIN H, et al. Microstructural evolution during non-isothermal annealing of a precipitation-hardenable aluminum alloy: Experiment and simulation [J]. Acta Materialia, 2015, 94: 111−123. DOI: 10.1016/j.actamat.2015.04.037.

[25] DEY G K. Physical metallurgy of nickel aluminides [J]. Sadhana, 2003, 28(1): 247−262. DOI: 10.1007/BF02717135.

[26] XIANG Z D, ROSE S R, DATTA P K. Long term oxidation resistance and thermal stability of Ni-aluminide/Fe-aluminide duplex diffusion coatings formed on ferritic steels at low temperatures [J]. Intermetallics, 2009, 17(6): 387−393. DOI: 10.1016/j.intermet.2008.11.009.

[27] JOZWIK P, POLKOWSKI W, BOJAR Z. Applications of Ni_3Al based intermetallic alloys—Current stage and potential perceptivities [J]. Materials, 2015, 8(5): 2537−2568. DOI: 10.3390/ma8052537.

[28] VISHWANATHA A D, PANDA B, SHIVANNA D M. Effect of a T6 aging treatment on the corrosion behaviour of in situ Al_xNi_y reinforced AA6061 composite [J]. Materials Today: Proceedings, 2021, 44: 4112 − 4117. DOI: 10.1016/j.matpr.2020.10.455.

[29] ABUTHAKIR J, SUBRAMANIAN R, KAVITHA M, et al. Corrosion studies of Al_x-Ni insitu intermetallics reinforced Al metal matrix composites [J]. Materials Today: Proceedings, 2020, 28: 1158−1163. DOI: 10.1016/j.matpr.2020.01.100.

[30] MONDOLFO L F. Aluminum alloys: Structure and properties [M]. Elsevier, 2013.

[31] RAHMATI Z, JAMSHIDI AVAL H, NOUROUZI S, et al. Effects of pre-heat treatment of the consumable rod on the microstructural and mechanical properties of the friction surfaced Al-Cu-Mg alloy over pure aluminum [J]. Surface and Coatings Technology, 2021, 410: 126954. DOI: 10.1016/j.surfcoat.2021.126954.

[32] BARARPOUR S M, JAMSHIDI AVAL H, JAMAATI R. Modeling and experimental investigation on friction surfacing of aluminum alloys [J]. Journal of Alloys and Compounds, 2019, 805: 57 − 68. DOI: 10.1016/j. jallcom.2019.07.010.

[33] HANKE S, DOS SANTOS J F. Comparative study of severe plastic deformation at elevated temperatures of two aluminium alloys during friction surfacing [J]. Journal of Materials Processing Technology, 2017, 247: 257−267. DOI: 10.1016/j.jmatprotec.2017.04.021.

[34] EHRICH J, ROOS A, KLUSEMANN B, et al. Influence of Mg content in Al alloys on processing characteristics and dynamically recrystallized microstructure of friction surfacing deposits [J]. Materials Science and Engineering A, 2021, 819: 141407. DOI: 10.1016/j.msea.2021.141407.

[35] HUMPHREYS F J, HATHERLY M. Recrystallization textures [M]// Recrystallization and Related Annealing Phenomena. Amsterdam: Elsevier, 1995: 327−362. DOI: 10.1016/b978-0-08-041884-1.50017-9.

[36] FARAJOLLAHI R, JAMSHIDI AVAL H, JAMAATI R. Evaluating of the microstructure, texture, and mechanical properties of AA2024-Al_3NiCu composites fabricated by the stir casting process [J]. CIRP Journal of Manufacturing Science and Technology, 2022, 37: 204−218. DOI: 10.1016/j.cirpj.2022.01.013.

[37] MORADI M M, JAMSHIDI AVAL H, JAMAATI R. Effect of pre and post welding heat treatment in SiC-fortified dissimilar AA6061-AA2024 FSW butt joint [J]. Journal of Manufacturing Processes, 2017, 30: 97−105. DOI: 10.1016/j.jmapro.2017.08.014.

[38] PIRHAYATI P, JAMSHIDI AVAL H, LOUREIRO A. Characterization of microstructure, corrosion, and tribological properties of a multilayered friction surfaced Al-

Mg-Si-Ag alloy [J]. Archives of Civil and Mechanical Engineering, 2022, 22(4): 1–14. DOI: 10.1007/s43452-022-00497-3.

[39] BARARPOUR S M, JAMSHIDI AVAL H, JAMAATI R. Mechanical alloying by friction surfacing process [J]. Materials Letters, 2019, 254: 394–397. DOI: 10.1016/j.matlet.2019.07.113.

[40] ABURADA T, ÜNLÜ N, FITZ-GERALD J M, et al. Effect of Ni as a minority alloying element on the corrosion behavior in Al-Cu-Mg-(Ni) metallic glasses [J]. Scripta Materialia, 2008, 58(8): 623−626. DOI: 10.1016/j.scriptamat.2007.11.041.

[41] CHEN Liang, HOU Yu-zhu, LI Zhi-gang, et al. Enhancing mechanical properties and corrosion resistance of a high strength 7A99 Al alloy by introducing pre-rolling in solution and aging treatments [J]. Journal of Alloys and Compounds, 2022, 898: 162972. DOI: 10.1016/j.jallcom.2021.162972.

[42] PAN T A, LIAN Yu-jia, TZENG Y C, et al. Effects of trace Ag and heat treatment on the mechanical properties and corrosion resistance of Al-Zn-Mg-Cu alloys [J]. JOM, 2022, 74(10): 3877−3886. DOI: 10.1007/s11837-022-05416-8.

[43] FARAJOLLAHI R, JAMSHIDI AVAL H, JAMAATI R, et al. Effects of pre- and post-friction surfacing heat treatment on microstructure and corrosion behavior of nickel-aluminide reinforced Al-Cu-Mg alloy [J]. Journal of Alloys and Compounds, 2022, 906: 164211. DOI: 10.1016/j.jallcom.2022.164211.

(Edited by ZHENG Yu-tong)

中文导读

镍铝化物增强摩擦堆焊Al-Cu-Mg合金基复合涂层的非等温时效行为

摘要：本文研究了镍铝化物对Al-Cu-Mg合金非等温时效行为的影响。对经非等温时效处理的含镍铝化物Al-Cu-Mg合金的组织、力学性能和耐蚀性进行了评价。结果表明，在Al-Cu-Mg基体中加入1.5 wt% Ni后，Al-Cu-Mg基体中镍铝化物的存在使析出物由S-Al_2CuMg转变为θ-Al_2Cu。在非等温时效过程中，达到最大力学性能的非等温时效处理温度由250 ℃转变为300 ℃。与170 ℃等温人工时效处理相比，经非等温时效处理的含镍铝化物Al-Cu-Mg合金的最大硬度和力学性能均提高了9%。含镍铝化物试样在300 ℃时达到最大硬度和抗剪强度，分别为HV0.1(143.4±6.4)和(298.6±9.6) MPa。非等温时效处理后，与AA2024铝合金基体和不含镍铝化物涂层相比，含镍涂层的腐蚀电流强度分别降低了约58%和49%。与传统的人工时效处理相比，经非等温时效处理的含镍铝涂层的腐蚀电流降低了16.7%。

关键词：非等温时效；镍添加剂；摩擦堆焊；微观结构；腐蚀行为